Evidence for Asymmetric Electron Transfer in Cyanobacterial Photosystem I: Analysis of a Methionine-to-Leucine Mutation of the Ligand to the Primary Electron Acceptor A_0[†]

Rachel O. Cohen,[‡] Gaozhong Shen,[‡] John H. Golbeck,*[,‡] Wu Xu,[§] Parag R. Chitnis,[§] Alfia I. Valieva,[#] Art van der Est,*[,#] Yulia Pushkar,[⊥] and Dietmar Stehlik*[,⊥]

Department of Biochemistry and Molecular Biology, The Pennsylvania State University, University Park, Pennsylvania 16802, Department of Biochemistry, Biophysics, and Molecular Biology, Iowa State University, Ames, Iowa 50011, Department of Chemistry, Brock University, St. Catharines, Ontario, Canada L2S 3A1, and Fachbereich Physik, Freie Universität Berlin, Arnimallee 14, D14195 Berlin, Germany

Received September 10, 2003; Revised Manuscript Received February 17, 2004

ABSTRACT: The X-ray crystal structure of photosystem I (PS I) depicts six chlorophyll *a* molecules (in three pairs), two phylloquinones, and a [4Fe-4S] cluster arranged in two pseudo C_2-symmetric branches that diverge at the P_{700} special pair and reconverge at the interpolypeptide F_X cluster. At present, there is agreement that light-induced electron transfer proceeds via the PsaA branch, but there is conflicting evidence whether, and to what extent, the PsaB branch is active. This problem is addressed in cyanobacterial PS I by changing $Met688_{PsaA}$ and $Met668_{PsaB}$, which provide the axial ligands to the Mg^{2+} of the eC-A3 and eC-B3-chlorophylls, to Leu. The premise of the experiment is that alteration or removal of the ligand should alter the midpoint potential of the A_0^-/A_0 redox pair and thereby result in a change in the forward electron-transfer kinetics from A_0^- to A_1. In comparison with the wild type, the PsaA-branch mutant shows: (i) slower growth rates, higher light sensitivity, and reduced amounts of PS I; (ii) a reduced yield of electron transfer from P_{700} to the F_A/F_B iron-sulfur clusters at room temperature; (iii) an increased formation of the $^3P_{700}$ triplet state due to $P_{700}^+A_0^-$ recombination; and (iv) a change in the intensity and shape of the polarization patterns of the consecutive radical pair states $P_{700}^+A_1^-$ and $P_{700}^+F_X^-$. The latter changes are temperature dependent and most pronounced at 298 K. These results are interpreted as being due to disorder in the A_0 binding site, which leads to a distribution of lifetimes for A_0^- in the PsaA branch of cofactors. This allows a greater degree of singlet-triplet mixing during the lifetime of the radical pair $P_{700}^+A_0^-$, which changes the polarization patterns of $P_{700}^+A_1^-$ and $P_{700}^+F_X^-$. The lower quantum yield of electron transfer is also the likely cause of the physiological changes in this mutant. In contrast, the PsaB-branch mutant showed only minor changes in its physiological and spectroscopic properties. Because the environments of eC-A3 and eC-B3 are nearly identical, these results provide evidence for asymmetric electron-transfer activity primarily along the PsaA branch in cyanobacterial PS I.

Photosystem I (PS I)[1] is a light-driven plastocyanin/cytochrome c_6:ferredoxin/flavodoxin oxidoreductase present in the membranes of cyanobacteria and chloroplasts. Its most immediate function is to convert a photon into chemical bond energy in the form of NADPH. The enzyme contains 12 polypeptides in cyanobacteria, but the core is a heterodimer of the PsaA and PsaB polypeptides that contains the spectroscopically identified electron-transfer cofactors P_{700}, a chlorophyll *a*/*a*′ heterodimer; A_0, a chlorophyll *a* monomer; A_1, a phylloquinone; and F_X, a [4Fe-4S] cluster (for a review see ref *1*). The 2.5 Å resolution X-ray crystal structure (*2*) shows three pairs of chlorophyll *a* molecules and a pair of phylloquinones arranged in two pseudo C_2-symmetric branches that diverge at the chlorophyll *a*/*a*′ P_{700} heterodimer and converge at the interpolypeptide F_X cluster. It is assumed that one or both of the distal chlorophyll *a* molecules serves as the primary acceptor, A_0 with a bridging chlorophyll *a* molecule (A_{-1}) located between P_{700} and each A_0. However, the electron-transfer capability of these two possible pathways is still under debate. Evidence for two nearly equivalent branches has mainly been obtained for PS I of eukaryotes

[†] This work was supported by grants from the National Science Foundation (MCB-0117079 to J.H.G., MCB-0078264 to P.R.C.); the Deutsche Forschungsgemeinschaft (SFB 498, TPA3, and SPP 'High Field EPR' to D.S.); and NSERC, CFI, OIT and a Premier's Research Excellence Award (to A.vdE.).

* To whom correspondence should be addressed. Tel.: 814 865 1163. Fax: 814 863 7024. E-mail: JHG5@psu.edu (or avde@brocku.ca or stehlik@physik.fu-berlin.de).

[‡] The Pennsylvania State University.

[§] Iowa State University.

[#] Brock University.

[⊥] Freie Universität Berlin.

[1] Abbreviations: PS I, photosystem I; PS II, photosystem II; P_{700}, primary donor in PS I; A_0, primary chlorophyll acceptor in PS I; A_1, quinone acceptor in PS I; F_x, F_A and F_B, iron-sulfur clusters in PS I; Fe/S, unspecified iron-sulfur cluster; Chl, chlorophyll; NADPH, reduced form of nicotinimide adenine dinucleotide phosphate; PsaA, PsaB, etc., protein subunits of the PS I complex; Q_K-A, Q_K-B, phylloquinones bound to PsaA and PsaB; *β*-DM, *n*-dodecyl-*β*-D-maltopyranoside; WT, wild type; EPR, electron paramagnetic resonance; ENDOR, electron nuclear double resonance; E, emission; A, absorption.

10.1021/bi035633f CCC: $27.50
Published on Web 04/02/2004

such as the alga *Chlamydomonas reinhardtii* (*3*−*6*), while evidence for more asymmetric electron transfer in PS I has been obtained for prokaryotes such as the cyanobacteria *Synechocystis sp.* PCC 6803 and *Synechococcus* sp. PCC 7002 (*7*−*10*). There is agreement in the data from both organisms that the 200 ns phase of A_1^- to F_X electron transfer occurs in the PsaA branch of cofactors and that the radical pair $P_{700}^+A_1^-$ detected in transient EPR experiments involves the quinone in this branch. There is also agreement that the majority of the electron transfer proceeds via the PsaA-branch (*3*−*10*). At present, however, the extent to which the PsaB-branch is active in electron transfer remains an unsolved issue.

These conclusions about the electron-transfer pathway in PS I are based primarily on studies involving specific mutations around the respective phylloquinone binding sites on the PsaA and PsaB polypeptides (*3*−*5*, *7*−*9*). The advantage to these mutations is that the spectral and functional changes they induce are so minor that they are not expected to influence the initial charge separation. The disadvantage is that the subtle changes induced by the mutations leaves some ambiguity in the interpretation of the spectral data. We therefore decided to focus on constructing mutations at the A_0 site, which precedes A_1 in the electron-transfer chain. These mutations should have a more pronounced effect on the spectral data and should enable us to probe the electron-transfer properties at the level of primary charge separation. One complication arising from mutations in this region is that they may influence the initial charge separation and thereby force electron transfer down an otherwise inactive pathway. Indeed, evidence to this effect has been presented in a recent report of A_0 mutants in *C. reinhardtii* (*6*). However, by constructing identical, separate mutations on both the PsaA-side and the PsaB-side of the PS I complex, we expect any asymmetry in the electron-transfer pathway to be reflected in their phenotypes, i.e., if the electron transfer uses both branches we should obtain similar phenotypes for the two mutants, while if the electron transfer uses only one branch, we should obtain very different phenotypes for the two mutants.

The identity of A_0 is not known with absolute certainty, but it is clear that the chlorophyll *a* molecules referred to as eC-A3 and eC-B3 in the X-ray structure (*1*, *2*) precede the phylloquinones in the two possible electron-transfer chains. Thus, it is assumed that one or both of these chlorophylls represent A_0. To influence the properties of A_0, it is particularly attractive to make point mutations of the Met residues $M688_{PsaA}$ and $M668_{PsaB}$ that are proposed to provide the axial ligands to the respective Mg^{2+} ions of the two chlorophylls.[2] Regardless of the nature of the interaction between the Met and the chlorophylls, their proximity to one another means that a mutation will likely alter the midpoint potential of the A_0^-/A_0 redox pair. This should result in a change in Gibbs free energy associated with both the forward and back electron transfer from A_0^- due to a change in the Frank−Condon factor in the Marcus equation, which relates the rate of electron transfer to changes in free energy and reorganization energy (*11*). Several possible consequences of such a change can be expected. First, it may have a significant influence on the temperature dependence of the rates, since the activation energy for forward electron transfer from A_0 to A_1 is known to be small in native PS I. Second, depending on how the midpoint potential affects the electron-transfer rate, the recombination of $P700^+A_0^-$ to the $^3P_{700}$ triplet state may be able to compete with forward electron transfer. Consequently, the quantum yield of charge separation beyond A_0 may be reduced and the spin polarization patterns of the subsequent radical pairs $P700^+A_1^-$, and $P_{700}^+F_X^-$ may be altered. Finally, it is possible that the mutation may disrupt the local structure and induce a distribution of properties for A_0 and a combination of both effects may be observed.

Here, we report a physiological and spectroscopic characterization of Met-to-Leu point mutants of the putative A_0 binding sites in the PsaA and PsaB proteins of *Synechocystis* sp. PCC 6803. We will show that the mutation in the PsaA protein has a pronounced effect on the spectroscopic and physiological properties of the cyanobacterium, while the corresponding mutation in the PsaB protein does not show significant differences from the wild type apart from an alteration in the backreaction kinetics. The results suggest that forward electron transfer in cyanobacterial PS I is asymmetric and occurs predominantly along the PsaA-branch of electron-transfer cofactors.

MATERIALS AND METHODS

Mutagenesis of the psaA and psaB Genes. For site-directed mutagenesis of the *psaA* and *psaB* genes, the *Synechocystis* sp. PCC 6803 recipient strain pWX3 was constructed with deletion of part of the *psaA* gene or deletion of the whole *psaB* gene as described previously (*9*). To generate site-specific mutants in the *psaA* gene, the pIBC plasmid was constructed by cloning a DNA fragment containing the majority of *psaA*, *psaB*, and a 760-bp downstream region of the *psaB* gene into a pBluescript II KS vector. A chloramphenicol resistant cassette gene was inserted after the 3′ terminator of the *psaB* gene. To generate site-specific mutants in the *psaB* gene, the plasmid pBC+ was constructed by cloning 1588 bp of the *psaB* 3′ region and a 760-bp region downstream of the *psaB* into a pBluescript II KS vector. A chloramphenicol resistance gene was inserted at the *Eco*RI site just downstream of the *psaB* gene. The *Synechocystis* sp. PCC 6803 recipient strain, pCRTΔB (a gift from Drs. Jianping Yu and Lee McIntosh, Michigan State University), was used for site-directed mutagenesis of the *psaB* gene. PCR mutagenesis was carried out using the Transformer site-directed mutagenesis kit (CLONTECH Laboratories, Inc). The mutated plasmid constructs were verified by sequencing and were used to transform the *Synechocystis* sp. PCC 6803 recipient strains. Segregation of the transformants was carried out by screening for chloramphenicol resistance. Full segregation of the desired mutants was verified by PCR and sequencing as described previously (*9*).

Growth of the Cyanobacterial Strains. The wild type and mutant strains of *Synechocystis* sp. PCC 6803 were grown in BG11 medium. Liquid cultures were supplemented with 1% CO_2. Illumination was provided by fluorescent lamps; the light intensity was raised or lowered by turning on or off individual lamps. The growth temperature was maintained

[2] The methionine ligand to Mg^{2+} is expected to be weak, and the possibility that an axial ligand is not required for binding of the chlorophyll may also have to be considered (*11*).

at 30 °C. The recipient strains pWX3 and pCRTΔB and the transformants could survive only in BG11 medium with addition of 5 mM glucose under conditions of light-activated heterotrophic growth (LAHG). Growth rates of the wild type and mutant strains were measured at various time points under photoautotrophic and photomixotrophic (with 5 mM glucose) growth conditions by monitoring the cells turbidometrically at 730 nm using a CARY-14 spectrophotometer modified for computerized data acquisition by On-Line Instruments.

Isolation of Thylakoid Membranes and PS I Trimers. Thylakoid membranes were prepared from the cyanobacterial cells by centrifugation. The cell pellets were washed once in 50 mm Tris/HCl, pH 8.0 and broken by three passages through a French pressure cell operating at 20 000 lb/in^2 at 4 °C. Unbroken cells and debris were removed by centrifugation at 5000*g* for 10 min at 4 °C. The thylakoid membranes were pelleted by centrifugation at 50000*g* for 45 min, and resuspended to a chlorophyll concentration of 1 mg/mL in 50 mM HEPES/NaOH, pH 8.0, containing 5 mM $MgCl_2$, 10 mM $CaCl_2$, 0.5% (v/v) dimethyl sulfoxide, and 15% (v/v) glycerol for storage, or, alternatively, in 50 mM Tris/HCl, pH 8.0 for preparation of PS I complexes. The isolation of PS I complexes was carried out according to the procedure of Shen et al. (*12*). In brief, thylakoid membranes were solubilized in *n*-dodecyl-β-D-maltoside (β-DM) and purified on two sucrose density gradients. The trimeric PS I complexes were present in the bottom green band and resuspended in 50 mM Tris, pH 8.0 containing 0.03% β-DM and 15% glycerol.

Chlorophyll, Carotenoid, Phylloquinone and Iron Sulfur Cluster Analysis. Chlorophylls and carotenoids were extracted from whole cyanobacterial cells with 100% methanol and from thylakoids with 80% acetone. The optical density was measured using a Cary 14 spectrophotometer. The chlorophyll concentration was determined according to Mackinney (*13*) and Lichtenthaler (*14*). The crude carotenoid content was measured based on the methods described by Hirschberg and Chamovitz (*15*). The phylloquinone content of PS I complexes was determined by HPLC and optical detection according to ref *16*. The presence of iron−sulfur clusters F_A and F_B in the PS I trimers was determined by CW-EPR spectroscopy after illuminating the sample at cryogenic temperatures (data not shown).

Low-Temperature Fluorescence Spectroscopy. Fluorescence emission spectra of the wild type and mutant cyanobacterial cells were measured at 77 K using a SLM 8000C spectrofluorometer as described (*12*). Exponential growth cells (monitored at $OD_{730} = 0.6-0.7$) were collected and resuspended in 25 mM HEPES/NaOH buffer, pH 7. Cells were diluted in 25 mM HEPES/NaOH buffer, pH 7, with 60% (v/v) glycerol to a concentration of 1 OD_{730} per mL prior to freezing in liquid nitrogen. The excitation wavelength was 440 nm for chlorophyll excitation. A long pass filter (cut-off at 600 nm) was used at the inlet of the emission monochromator to minimize contributions from scattered light.

Room-Temperature Optical Kinetic Spectroscopy in the Near-IR Region. Transient absorbance changes in the near-IR were measured in PS I complexes using a laboratory-built double-beam spectrophotometer. The sample was prepared anaerobically and placed in a 10 × 4-mm quartz cuvette with an airtight stopper. The excitation beam was provided by a frequency-doubled ($\lambda = 532$ nm), Q-switched Nd:YAG laser (DCR-11, Spectra Physics, Mountain View, CA) and expanded to a diameter of 15 mm and oriented normal to the longer side of the 5 × 10 mm cuvette. The pulse width at half-maximum was 10 ns, and the flash energy was attenuated by varying the Q-switch delay and using a combination of neutral density filters. The 820 nm measuring beam was provided by semiconductor diode laser (Spindler & Hoyer GmbH & Co., Göttingen, Germany) and was oriented normal to the shorter side of the 5 × 10 mm cuvette. The measuring beam was divided with a 1:1 ratio nonpolarizing broadband beam splitter; the signal beam was passed through the cuvette, while the reference beam was passed through a variable-density filter wheel to equalize the intensities of the two beams. Both beams were converted into photocurrents using a pair of reverse-biased silicon photodiodes (model PIN-10D, United Detector Technology, Hawthorne, CA) shielded by cutoff filters (RG-10, Schott Glas, Mainz, Germany). The photocurrents were converted into voltages with 100-Ohm resistors, and the difference between the signal and reference voltage was analyzed in real time at 8-bit vertical resolution using a 150-MHz bandwidth DC-coupled differential comparator (model 11A33, Tektronix Inc., Beaverton, OR) plugged into a digital signal analyzer (model DSA 601, Tektronix, Inc., Beaverton, OR). PS I trimers isolated from *Synechocystis* sp. PCC 6803 were suspended at 50 μg/mL Chl in 25 mM Tris-HCl buffer, pH 8.3, 10 mM Na ascorbate, 4 μM 2,6-dichlorophenolindophenol (DPIP), and 0.04% β-DM. The ΔA_{820} kinetics were fitted using a stretched exponential algorithm (see ref *17*) that was programmed in IGOR Pro v. 4.4 (Wavemetrics, Lake Oswego, OR). A stretched exponential minimizes the number of closely spaced kinetic components while preserving the most significant kinetic features of the spectrum. It is based on the premise that a distribution of closely spaced kinetic phases occurs due to microheterogeneity or conformational flexibility within large protein structures. A stretch factor of 1.0 represents a monotonic decay.

Room-Temperature Optical Kinetic Spectroscopy in the Visible Region. Flash-induced absorbance changes in the visible region were measured at room temperature using a pump−probe spectrophotometer constructed by Ilya Vassiliev and one of the authors (J. Golbeck). The spectrometer is based on a design by Joliot et al. (*18*) but modified so that the signals are digitized as stored waveforms prior to integration. The optical path consists of a xenon flash (model 9650, EG&G, Gaithersburg, MD), a 3/4 m monochromator (model HO439, Bausch & Lomb, Rochester, NY) outfitted with a grating blazed at 350 nm, and a light scrambling chamber designed by Kramer and Sacksteder (*19*). The scrambling chamber, which is similar to an integrating sphere, was milled from Spectralon (Labsphere, North Sutton, NH), and constructed with an entry port and two output ports outfitted with a nonimaging optical element termed a compound parabolic concentrator. The sample is placed in 1 × 1 cm cuvettes in the sample and reference arms; an OPO-based pump laser (model VIBRANT 355 II, Opotek Corp.) excites the sample arm at 5 mJ cm^{-2} of flash energy and at a wavelength of 686 nm. The detectors are protected against the pump pulse using a pair of cyan dichroic filters (F52−537, Edmund Scientific Optics). At a variable

time after the actinic flash, the xenon probe is fired; the light-induced signal is detected using two matched PIN photodiodes (model PIN-10D, United Detector Technology, Hawthorne, CA) and fed into a differential comparator (model 11A33, Tektronix Inc., Beaverton, OR) plug-in of a digital signal analyzer (model DSA 601, Tektronix, Inc., Beaverton, OR). Separately, the sample and reference signals are fed into third and fourth channels of the digital signal analyzer using a 600 MHz plug-in (model 11A52, Tektronix Inc., Beaverton, OR), and the trigger is captured using a photodiode (model PIN-10D, United Detector Technology, Hawthorne, CA) fed into a fifth channel of the digital signal analyzer using a 300 MHz plug-in (model 11A32, Tektronix Inc., Beaverton, OR). The digital signal analyzer captures the entire waveform produced by the difference and the reference channels and the two waveforms are ported to a Power Macintosh computer via a IEEE-488 bus (model PCI-GPIB, National Instruments, Austin, TX) for signal processing. Laboratory-constructed software written in IGOR Pro v. 4.4 (Wavemetrics, Inc., Lake Oswego, OR) controls the spacing between the pump and probe flashes with a programmable pulse generator (model 8112A, Hewlett-Packard Co., Palo Alto, CA), and provides a user interface for command and control of the spectrometer. The software integrates the difference waveform and the reference waveform, calculates the absorbance change, and plots the results on a logarithmic scale. The software allows signal averaging up to 1024 separate flashes. The spectrometer has an S/N better than 10^{-5} Å at 400 nm and a temporal resolution of 2 μs between 390 and 600 nm. Decay-associated spectra are extracted from a global decomposition of the kinetic data using an algorithm written in IGOR Pro 4.4 (Wavemetrics, Inc., Lake Oswego, OR).

Variable Temperature X-Band Transient EPR Spectroscopy. X-band transient EPR experiments were carried out using a microwave bridge (model ER046 XK-T, Bruker BioSpin GmbH, Rheinstetten, Germany) equipped with a Flexline dielectric resonator (*20*) and a liquid helium gas-flow cryostat (Oxford Instruments, Whitney, Oxfordhsire, UK) to cover the temperature range between 80 and 260 K. All samples contained 1 mM sodium ascorbate and 50 μM phenazine methosulfate as external redox agents and were frozen in the dark. The pulsed light source for the experiments was a Q-switched, frequency-doubled Nd:YAG laser (model GCR 130 Spectra Physics, Mountain View, CA) operating at $\lambda = 532$ nm with a pulse width of 8 ns and a variable repetition rate operating typically at 10 Hz. Selected checks were performed using lower repetition rate of 1 Hz, especially at higher temperatures around 260 K. No change in signal intensity was found for repetition rates less than 10 Hz, which is consistent with the expected kinetics of the external redox agents.

Room-Temperature X-Band Transient EPR Spectroscopy. Room temperature X-band EPR experiments were performed using a modified Bruker ESP 200 spectrometer equipped with a home-built, broadband amplifier (bandwidth > 500 MHz). A flat cell and a rectangular resonator were used, and the samples were illuminated using a Q-switched, frequency doubled Continuum Surelite Nd:YAG laser at 532 nm with a repetition rate of 10 Hz. The external donors sodium ascorbate (1 mM) and phenazine methosulfate (50 μM) were added to mediate electron transport.

Table 1: Physiological Characteristics of the *Synechocystis* 6803 Wild-Type and Mutant Strains

	photoautotrophic growth doubling time at normal light (h)	photoautotrophic growth doubling time at higher light (h)	chlorophyll content (μg of Chl/OD_{730})	phylloquinone (per 96 chlorophyll molecules)[a]
wild type	17 ± 0.7	23 ± 1.1	3.6 ± 0.3	1.95 ± 0.07
$M668L_{PsaB}$	19 ± 0.6	27 ± 0.8	3.1 ± 0.2	1.86 ± 0.06
$M688L_{PsaA}$	26 ± 0.9	38 ± 1.3	2.4 ± 0.2	2.04 ± 0.08

[a] Average of four independent measurements.

RESULTS

Physiological Characterization of the $M688L_{PsaA}$ and $M668L_{PsaB}$ Mutant Strains. The mutant strains were constructed by replacing $M684_{PsaA}$ or $M659_{PsaB}$ in *Synechocystis* sp. PCC 6803 with a Leu residue. To maintain a consistent nomenclature between species, we will henceforth use the numbering system of amino acids in PS I from *Thermosynechococcus elongatus*, for which the X-ray crystal structure has been solved (*2*). Thus, in this work, $M688L_{PsaA}$ is the PsaA-side mutant and $M668L_{PsaB}$ is the PsaB-side mutant. The mutations were confirmed by sequencing the amplified DNA fragments containing the mutation sites from the genomic DNA. As shown in Table 1, the $M688L_{PsaA}$ and $M668L_{PsaB}$ cells were capable of growing on light alone (photoautotrophic growth). However, the $M688L_{PsaA}$ cells showed a consistently longer doubling time (26 h) at "normal" light intensities (100 μE m^{-2} s^{-1}) than either the $M668L_{PsaB}$ cells (19 h) or the wild type (17 h). At higher light intensities (300 μE m^{-2} s^{-1}), the $M688L_{PsaA}$ cells were increasingly sensitive when compared to the $M668L_{PsaB}$ cells or the wild type.

Under iron-replete conditions, the chlorophyll molecules in cyanobacteria are associated primarily with the PS I and PS II reaction centers. Thus, the chlorophyll content of whole cells reflects the overall amounts of PS I and PS II in the membranes. As listed in Table 1, the amount of chlorophyll was slightly reduced in the $M668L_{PsaB}$ cells compared to the wild-type cells, but the amount of chlorophyll was significantly lower in the $M688L_{PsaA}$ cells. This result implies that there is a lower steady-state level of PS I when the mutation is made on the PsaA-side than on the PsaB-side due to either lower overall assembly or higher overall disassembly (or both) of PS I reaction centers. On the basis of a comparison of the chlorophyll content and PS II quantitation by a herbicide-binding assay, the PS I to PS II ratio is estimated to be 5-to-1 in the wild-type strain of *Synechocystis* sp. PCC 6803 (*21*). Because the majority of chlorophyll in cyanobacterial cells is associated with PS I, the amount of PS I is therefore likely to be lower in the $M688L_{PsaA}$ mutant cells than in the $M668L_{PsaB}$ mutant cells.

The lower ratio of PS I to PS II was confirmed by measuring on a basis of the same cell number the amplitude of the fluorescence emission in whole cells at 77 K. The 725 nm peak is derived largely from PS I, while the 685 and 695 nm peaks are derived largely from PS II. As shown in Figure 1, the fluorescence emission signal from the PS I-associated chlorophyll is lower in thylakoids from the two mutant strains than in the wild type. However, the amount of PS I, based on its fluorescence amplitude at 725 nm, is

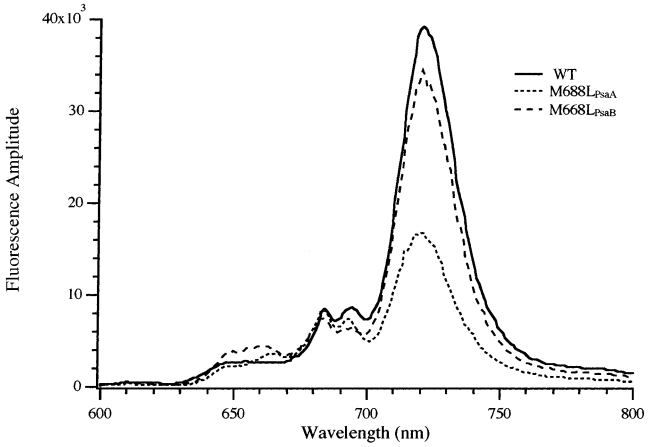

FIGURE 1: Fluorescence emission spectra at 77 K of whole cells of *Synechocystis* sp. PCC 6803 wild type (solid line), the M688L_{PsaA} mutant (dotted line), and the M668L_{PsaB} mutant (dashed line). Each spectrum is the average of five independent measurements. The excitation wavelength was 440 nm.

significantly reduced in thylakoids from the M688L_{PsaA} mutant cells as compared to the M668L_{PsaB} mutant cells. Thus, although there are no significant differences in the environments of the PsaA-side and PsaB-side chlorophylls, there is a difference in the amount of PS I in the two mutants.

PS I complexes from the wild type, the M688L_{PsaA} mutant, and the M668L_{PsaB} mutant contained on average 1.95, 1.86, and 2.04 molecules of phylloquinone per 96 chlorophylls, respectively (Table 1). Thus, the Met-to-Leu mutation in the vicinity of the A_0 chlorophylls does not lead to the loss of the phylloquinone from PS I.

Room-Temperature Flash-Induced Absorbance Changes in the Near-IR. Figure 2 shows a comparison of the flash-induced absorbance changes at 820 nm in PS I complexes isolated from the wild type (top), the M668L_{PsaB} mutant (middle), and the M688L_{PsaA} mutant (bottom). In PS I, a single turnover flash induces a bleaching in the near-IR followed by a decay. The bleaching results from the loss of ground-state character in chlorophyll due to the formation of a cation, an anion or a triplet state. These states can be distinguished by analysis of the light saturation characteristics and by the spectrum in the near-IR. If the light-induced absorbance change is due to photochemical charge separation, then the ΔA at 820 nm can be used to determine the yield of P_{700}^+ formation, and an analysis of the decay kinetics can provide a tentative identification of the electron acceptor from which recombination occurs. The decay of the flash-induced absorbance change at 820 nm is shown in Figure 2 for the wild type and the two mutants. As is immediately apparent from Figure 2, the two mutants differ significantly from each other and from the wild type.

For the wild type (Figure 2, top), the decay is biphasic with lifetimes (and stretch factors) of ca. 120 ms (0.74) and 1.0 s (0.67). The 120-ms kinetic phase is saturated at a flash intensity of 3.5 mJ cm^{-2} and is sensitive to methyl viologen concentration; it is tentatively assigned to recombination between P_{700}^+ and the terminal iron−sulfur clusters $[F_A/F_B]^-$ (*22*). The 1.0 s kinetic phase is sensitive to DPIP concentration and is ascribed to forward electron donation to P_{700}^+ in PS I complexes in which the electron has been lost from the terminal acceptors. The total absorbance change is 4.5 mOD; using an extinction coefficient of 8000 M^{-1} cm^{-1} at 820 nm

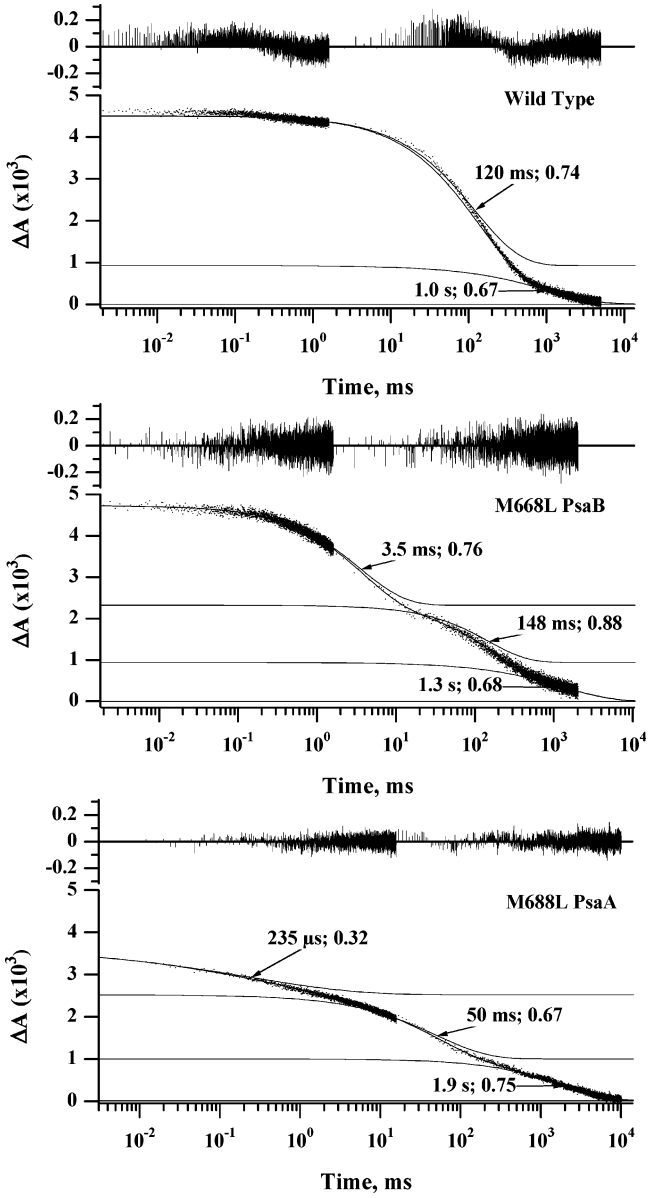

FIGURE 2: P_{700} decay kinetics of flash-induced absorbance changes at 820 nm of PS I complexes isolated from *Synechocystis* sp. PCC 6803 wild type (top), M668L_{PsaB} (middle), and M688L_{PsaA} (bottom) mutants. The samples contain 50 μg/mL chlorophyll in 25 mM Tris (pH 8.3), 10 mM sodium ascorbate, 4 μM DPIP, and 0.04% β-DM. The plots depict an average of 16 traces acquired at 10 s intervals. Time is plotted on a logarithmic scale in which a deviation from the horizontal represents a kinetic phase. The computer-generated exponential fit is shown as a solid line. Results of the exponential fits are displayed as fit curves (thin line). Each individual component is plotted with vertical offset relative to the next component (with a longer lifetime) or the baseline, the offset being equal to the amplitude of the latter component. The relative contributions of each kinetic phase can be judged by the intersection of the fit line with the abscissa. The residual of the fit is depicted above the main trace.

for P_{700}/P_{700}^+ (*23*), this is equivalent to 0.56 μM in P_{700} (50 μg mL^{-1} Chl) and corresponds to 100 Chl/P_{700} (0.96 P_{700}^+/PS I). This value agrees well with the expected value of 96 Chl/P_{700} determined from the X-ray crystal structure (*2*).

For both mutants (Figure 2, middle and bottom) multiphasic decay kinetics are observed, with the majority of absorbance change decaying faster than in the wild type. For the M668L_{PsaB} mutant (Figure 2, middle) the fit yields lifetimes (and stretch factors) of ca. 3.5 ms (0.76), 148 ms

(0.88), and 1.3 s (0.68). The amplitudes of the 3.5 and 148 ms kinetic phases are saturated at a flash intensity of 3.5 mJ cm^{-2} and are sensitive to methyl viologen concentration; both are tentatively assigned to the backreaction of P_{700}^+ with reduced iron-sulfur clusters. As in the wild type, a minor kinetic phase with a lifetime of 1.3 s, which is sensitive to DPIP concentration, is present and is ascribed to forward electron donation to P_{700}^+. The total absorbance change is 4.7 mOD, which is equivalent to 0.59 μM P_{700} (50 μg mL^{-1} Chl) and corresponds to 95 Chl/P_{700} (1.01 P_{700}^+/PS I), a value similar to the wild type. Thus, although the PsaB-side mutant shows altered recombination kinetics (which will be described in detail in a forthcoming paper), it is fully competent in long-lived charge separation to the iron−sulfur clusters.

For the $M688L_{PsaA}$ mutant (Figure 2, bottom) lifetimes (and stretch factors) of 235 μs (0.32), 50 ms (0.67), and 1.9 s (0.75) are obtained. The 50-ms kinetic phase is assigned to the backreaction of P_{700}^+, with the reduced iron−sulfur clusters because it saturates at a flash energy of 3.7 mJ cm^{-2} and is sensitive to methyl viologen concentration. The minor kinetic phase with a lifetime of 1.9 s is ascribed to forward electron donation to P_{700}^+ because it is sensitive to DPIP concentration. In contrast, the amplitude of the 235 μs kinetic phase does not saturate with laser flash energy up to 80 mJ cm^{-2}; additional kinetic components with lifetimes of ca. 0.3−0.4 ms and ca. 10 μs also appear at flash energies above 5 mJ cm^{-2}. We assign these two components to antenna processes, the faster of which is likely the decay of a chlorophyll triplet. The total absorbance change assigned to photochemical charge separation is 2.5 mOD, which is equivalent to 0.31 μM P_{700} (50 μg mL^{-1} Chl) and corresponds to 179 Chl/P_{700} (0.54 P_{700}^+/PS I). This value is nearly a factor of 2 lower than that found in the wild type and the PsaB-side mutant. Thus, in addition to altered rates of charge recombination between P_{700} and the iron-sulfur clusters, long-lived charge separation to the iron-sulfur clusters is generated in only about 50% of the PS I complexes in the PsaA-side mutant.

Room-Temperature Flash-Induced Absorbance Changes in the Visible. These assessments are corroborated by analysis of the flash-induced difference spectra in the visible region. Figure 3 shows decay-associated spectra of kinetic components obtained from a global decomposition of flash-induced transients recorded every 10 nm from 390 to 580 nm. In wild type PS I, the most prominent kinetic component has a lifetime of 130 ms, which correlates with the 120-ms kinetic component measured in the near-IR. The visible spectrum associated with this component (Figure 3, top, solid circles) has a minimum at 435 nm, a small absorbance increase at 445 nm, and is relatively featureless up to 580 nm. This spectrum is similar to the combined difference spectra of P_{700}/P_{700}^+ and $[Fe/S]/[Fe/S]^-$ (see Figure 2a in ref *24*) and is assigned to the backreaction of P_{700}^+ and $[F_A/F_B]^-$. Using a differential extinction coefficient at 435 nm of 44 000 mM^{-1} cm^{-1} for P_{700}/P_{700}^+ (*23*) and assuming a differential extinction coefficient of 5000 mM^{-1} cm^{-1} for $[Fe/S]/[Fe/S]^-$, the total absorbance change of 5.2 mOD is equivalent to 0.106 μM in P_{700}^+ and $[Fe/S]^-$ (10 μg mL^{-1} Chl) and corresponds to 106 Chl/P_{700} (0.91 P_{700}^+/PS I). The absorbance change of the comparable 120-ms kinetic component in the near-IR is 3.6 mOD, which is equivalent to 0.450 μM in P_{700} (50 μg mL^{-1} Chl) and corresponds to 124 Chl/P_{700} (0.77 P_{700}^+/PS I). Considering that the population of P_{700}^+ ascribed to forward electron donation from DPIP in the near-IR is not resolved in the global decomposition of the visible data, the data from the two spectral regions are in good agreement.

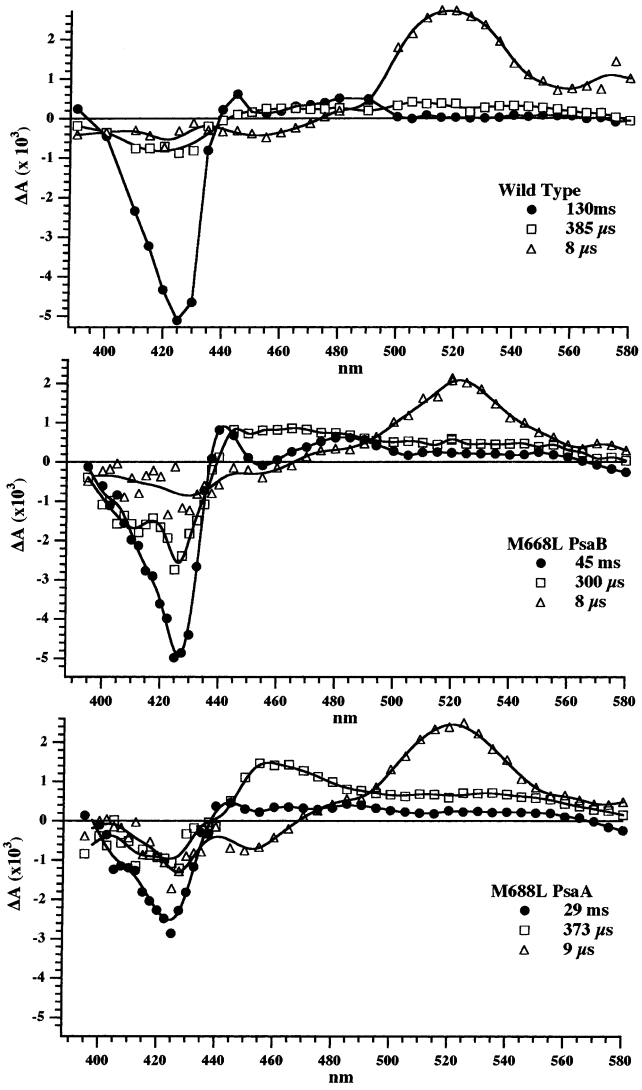

FIGURE 3: Global decomposition of optical kinetic transients in the visible region for the wild type (top), the $M668L_{PsaB}$ mutant (middle), and the $M688L_{PsaA}$ mutant (bottom). Conditions are similar to those of Figure 2 except that the samples contain 10 μg mL^{-1} chlorophyll. The kinetics were analyzed initially assuming the presence of either three components or two components and a baseline. The results of these analyses were then used for fitting the whole set of data to global lifetimes, and the best solution was chosen based on the analysis of χ^2, standard errors of the parameters, and the residuals of the fits.

The data in the visible also reveal two additional kinetic components with lifetimes of 385 and 8 μs, which are not observed at 820 nm. The spectrum associated with the 385 μs decay phase (open squares) shows only weak absorbance changes with a minimum around 430 nm and no peak at 445 nm. A crossover occurs around 440 nm, leading to a derivative-like spectrum that is reminiscent of an electrochromic bandshift. The weak featureless spectrum does not allow this component to be assigned with any degree of confidence. The spectrum associated with the 8 μs decay phase (open triangles) shows a moderately large, positive absorbance change centered at 520 nm and two small bleaching bands at 420 and 436 nm with a crossover at 470

nm. This spectrum strongly resembles a carotenoid triplet state (*25*). Since the sample was excited at 686 nm, the carotenoid triplet is most likely populated by triplet−triplet transfer from an antenna chlorophyll triplet (see also "EPR detected triplet states" below). Using an extinction coefficient for ^{3}Car/Car of 242 000 M^{-1} cm^{-1} at 515 nm taken from pulse radiolysis measurements of β-carotene in hexane (*26*), the absorbance change of 2.5 mOD is equivalent to 1080 Chl/^{3}Car and corresponds to 0.088 ^{3}Car/P_{700}. Thus, even though the change in optical density is large, the carotenoid triplet yield is relatively low in wild-type PS I complexes.

In the M668L_{PsaB} mutant (Figure 3, middle), the decay-associated spectra are similar to the wild type. The spectrum associated with the kinetic lifetime of 45 ms (solid circles) has a minimum at 435 nm, a small absorbance increase at 445 nm, and is relatively featureless to 580 nm. It is similar to the combined difference spectra of P_{700}/P_{700}^+ and $[Fe/S]/[Fe/S]^-$ observed in the wild type. Although the data in the near-IR show two kinetic components of 3.5 and 148 ms, the global decomposition of the visible data resolves only a single kinetic component with a lifetime of 45 ms, a value similar to the weighted average of 46 ms from the near-IR measurement. (The kinetics were analyzed assuming the presence of either three components or two components and a baseline.) The total absorbance change of 5.0 mOD is equivalent to 0.102 μM in P_{700}^+ and $[Fe/S]^-$ (10 μg mL^{-1} Chl) and corresponds to 110 Chl/P_{700} (0.87 P_{700}^+/PS I). The total absorbance change of the comparable 3.5 and 148 ms components in the near-IR is 3.75 mOD, which is equivalent to 0.469 μM in P_{700} (50 μg mL^{-1} Chl) and corresponds to 119 Chl/P_{700} (0.81 P_{700}^+/PS I). Hence, the data from the visible are in good agreement with the data from the near-IR.

The spectrum associated with the 300 μs decay phase (open squares) is more pronounced than in the wild type, showing a similar bleaching at 425 nm, a crossover at 440 nm, and a relatively unstructured absorbance increase extending to 560 nm. The absence of a peak at 440 nm and a trough at 455 nm rules out a contribution from the P_{700}/P_{700}^+ difference spectrum. Again, this derivative-like spectrum is reminiscent of an electrochromic bandshift, but otherwise it remains unassigned. The spectrum associated with the 8 μs decay phase (open triangles) is similar to the corresponding spectrum from wild type, showing bleaching bands at 425 and 455 nm, a crossover at 470 nm, and a peak at 520 nm, and is assigned to a carotenoid triplet.

In the M688L_{PsaA} mutant (Figure 3, bottom), the decay-associated spectra are similar to the other two samples, but the amplitude of the 29-ms component (solid circles) is diminished. The spectrum of this component resembles the combined difference spectra of P_{700}/P_{700}^+ and $[Fe/S]/[Fe/S]^-$ observed in the wild type with a minimum at 435 nm, a small absorbance increase at 445 nm, and a relatively featureless region to 580 nm. The total absorbance change of 2.5 mOD is equivalent to 0.051 μM in $P700^+$ and $[Fe/S]^-$ (10 μg mL^{-1} Chl) and corresponds to 220 Chl/P_{700} (0.43 P_{700}^+/PS I). The absorbance change of the comparable 50-ms component in the near-IR is 1.5 mOD, which is equivalent to 0.188 μM in P700 (50 μg mL^{-1} Chl) and corresponds to 299 Chl/P_{700} (0.32 P_{700}^+/PS I). Thus, the data from the visible show the same trend as the data from the near-IR.

The spectrum associated with the 373 μs phase (open squares) is similar to the PsaB-side mutant and the wild type, showing a broad bleaching around 420 nm, a crossover at 440 nm, and a broad peak around 455 nm, with a gradual decline to 570 nm. The absence of the peak at 440 nm and the trough at 455 nm rules out a contribution from the P_{700}/P_{700}^+ difference spectrum; while this spectral component is unassigned, we note that its amplitude is greater for both mutants in comparison to wild type. The spectrum associated with the 9 μs decay phase (open triangles) is also similar to the wild type, with bleaching bands at 425 and 455 nm, a crossover at 470 nm, and a peak at 520 nm, and is identified as a carotenoid triplet. The ^{3}Car triplet yield is therefore not affected by the mutation in either of the A_0 sites, consistent with triplet-triplet transfer from an antenna chlorophyll triplet.

Together, the initial amplitudes, kinetics, and the saturation behavior of the absorbance changes suggest that the PsaA-side mutation results in lower yield of charge separation between P_{700} and the iron sulfur clusters compared to the wild type or the PsaB-side mutant. We tentatively propose that the lower yield in the A-side mutant occurs because the electron is not transferred beyond A_0^- in about 50% of the PS I complexes. Since this fraction does not contribute to the absorbance changes, charge recombination would likely occur between P_{700}^+ and A_0^- to the ground state.

Forward Electron-Transfer Kinetics Through A_1. Transient EPR spectroscopy allows the kinetics of forward electron transfer from A_0^- through A_1 to F_X to be determined. The first of the two electron transfer steps involved cannot be resolved directly, but the polarization pattern of each radical pair in a sequential series such as $P_{700}^+A_0^-$, $P_{700}^+A_1^-$, and $P_{700}^+F_X^-$ depends on the spin evolution in all previous pairs. Thus, the polarization patterns of $P_{700}^+A_1^-$ and $P_{700}^+F_X^-$ are sensitive to changes in the lifetime of $P_{700}^+A_0^-$ provided they occur in the appropriate time range. Figure 4 shows room temperature kinetic traces for the wild type and the M688L_{PsaA} and M668L_{PsaB} mutants taken at the two field positions indicated by the arrows under the corresponding spectra on the left side of Figure 5. The solid curves in Figure 4 are fits to the data as described in ref *27*. On the low field side of the spectrum (position a; Figure 4, left) the signal is primarily due to $P_{700}^+A_1^-$ and the signal decay is dominated by the lifetime of A_1^-. Clearly, neither of the mutations in the A_0 site has a significant effect on the rate of forward electron transfer from A_1^- to F_X at room temperature. Moreover, the characteristic temperature dependence of this thermally activated rate (*8*, *28*, *29*) is also unaffected (data not shown). The fits in Figure 4 yield an electron-transfer time constant of 240 ns at ambient temperature, in good agreement with the kinetics determined for wild type. However, it is also apparent that although the kinetics are not changed, the transient at position b (Figure 4, right) and the corresponding polarization pattern in Figure 5, left, bottom, PsaA-side mutant) differ dramatically from those of the other two samples. A minor contribution from the late signal is also seen as a slow decay in the transient at position a from the PsaA mutant. The changes in the polarization pattern of the M688L_{PsaA} mutant can be explained qualitatively as a result of singlet−triplet mixing due to an increase in the lifetime of the primary radical pair $P_{700}^+A_0^-$. This effect is expected to produce equal and opposite net polarizations of A_1^- and P_{700}^+ with A_1^- in emission and P_{700}^+ in absorption. In accordance with this, the low-field half of

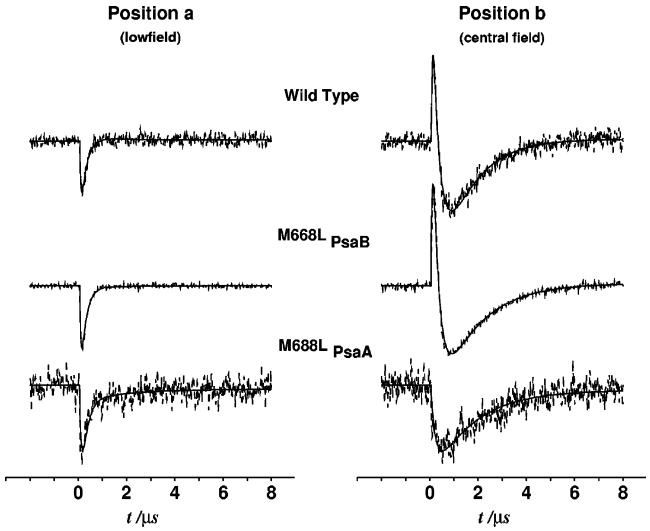

FIGURE 4: Room temperature spin polarized EPR transients of PS I complexes from the wild type (top), M668L$_{PsaB}$ (middle), and M688L$_{PsaA}$ (bottom) mutants. The transients on the left and right of the figure correspond to the field positions a and b marked by arrows under the spectra on the left of Figure 5. The solid curves are fits to the experimental transients using a model, which assumes a single kinetic phase corresponding to electron transfer from A_1^- to F_X. The fit yields a lifetime of 240 ± 50 ns for the electron transfer in all three samples.

the early spectrum of the PsaA-side mutant (solid curve Figure 5, bottom left) is emissive while the high-field half is absorptive. The subsequent electron transfer from A_1 to F_X then generates net emissive polarization of P_{700}^+ as seen for the late spectra of the wild type and PsaB-side mutant (dashed curves Figure 5 left, top and middle). In contrast, for the PsaA-side mutant the late spectrum (dashed curve Figure 5 left, bottom) shows roughly equal emissive and absorptive contributions to the spin polarization as a result of efficient singlet−triplet mixing in the $P_{700}^+A_0^-$ state.

From this we can draw the following conclusions: (i) as expected, neither of the two mutations affects the electron-transfer kinetics from A_1^- to F_X since they are not in the vicinity of either A_1 or F_X, and (ii) the spin polarization patterns associated with $P_{700}^+A_1^-$ and $P_{700}^+F_X^-$ are unaffected in the PsaB-side mutation (Figure 4, middle) but are strongly affected in the PsaA-side mutant (Figure 4, bottom) probably as a result of an increase in the lifetime of A_0^-.

Observation of $^3P_{700}$ due to Charge Recombination by Time-Resolved EPR Spectroscopy. In photosynthetic reaction centers, the triplet state of the primary donor (^{3}P) generated by charge recombination has a transient EPR spectrum with a characteristic spin polarization pattern (*30*). In PS I, when forward electron transfer passed A_0 is blocked, such a pattern is observed for $^3P_{700}$ (*31*) which has a characteristic temperature dependence due to delocalization of the triplet over the two chlorophylls of the P_{700} dimer (*32*). Thus, the spin polarized $^3P_{700}$ spectrum provides an additional indicator for alteration of forward electron transfer by the mutations. To confirm the presence or absence of triplet states, the right side of Figure 5 shows a comparison of X-band transient EPR spectra taken at 80 K over an appropriately wider field range than in the left side of Figure 5. The wild type and the M668L$_{PsaB}$ mutant (Figure 5 right, top and middle) show only minor but similar background signals in the wings of the spectra. The spectra are dominated by the strong off-scale signals at the center of the spectra due to $P_{700}^+A_1^-$. In sharp contrast, the M688L$_{PsaA}$ mutant shows a sizable contribution from the broad spectrum of $^3P_{700}$. The observed polarization pattern (A/E/E/A/A/E, A = absorption, E = emission) is a result of exclusive population of the T_0 spin level and is unique to triplet states formed by radical pair recombination. It is incompatible with other pathways such as intersystem crossing (ISC). Thus, the polarization pattern serves as a fingerprint for $^3P_{700}$ formation by recombination from $P_{700}^+A_0^-$, (for a review see ref *30*). This is consistent with the idea that forward electron-transfer beyond A_0 is slowed in the PsaA-side mutant to an extent that charge recombination via $^3P_{700}$ can compete. The significance of this result is that it not only confirms that at low-temperature reversible electron transfer occurs in the PsaA-branch of cofactors, but it also suggests that when this pathway is slowed or blocked efficient forward electron transfer cannot be maintained by rerouting electrons along the PsaB-branch. It is important to note that the PS I complexes isolated from the M688L$_{PsaA}$ mutant still contain two phylloquinones per 96 chlorophylls. Moreover, incubation with 2-methyl-1,4 naphthoquinone (*33*) had no effect on the transient EPR signals. Hence, the observed $^3P_{700}$ signal in the PsaA-side mutant is not due to a partial loss of quinone from the A_1 site. The $^3P_{700}$ spectral amplitude decreases with increasing temperature and reaches the detection limit above about 200 K (data not shown). However, it is difficult to draw conclusions from this observation because the $^3P_{700}$ yield is known to be strongly temperature dependent (*25*).

Together, the room temperature and low-temperature data shown in Figures 4 and 5 provide strong evidence that all the observed transient EPR spectra arise from PS I complexes associated with electron transfer along the PsaA-branch of cofactors. This suggests that either: (i) the majority of electrons proceed down the PsaA-branch, or (ii) electron transfer in the PsaB-branch produces no significant radical pair spin polarization or triplet formation.

Temperature Dependence of the Radical Pair Spin Polarization. If the changes in the polarization patterns in the PsaA mutant are indeed due to a slowing of forward electron transfer through A_0, it is possible that the patterns will also be temperature dependent. This would be in contrast with the wild type for which the spin polarization patterns of $P_{700}^+A_1^-$ and $P_{700}^+F_X^-$ are essentially independent of temperature. Figure 6 shows the early and late spin polarization patterns of the M688L$_{PsaA}$ mutant at three selected temperatures between 295 and 240 K. The spectra are taken in time windows centered at 110 ns and 1.4 μs following the laser flash. Clearly, the polarization patterns in both time regions change with temperature. As the temperature is decreased, the changes in the spectra induced by the mutation become weaker. This can be seen, for example, by the fact that the strong absorptive upfield feature observed at 295 K (Figure 6, top left) is much weaker at 260 and 240 K (Figure 6, middle, bottom left). This is an unexpected result, since it implies an increasing triplet character of the radical pairs at higher temperature. Were this only due to singlet−triplet mixing during the lifetime of $P_{700}^+A_0^-$, it would imply slower electron transfer at higher temperatures, contrary to the increase in rate normally observed at higher temperature for such processes. Therefore, alternative explanations must be considered. Since the side chain of Leu is somewhat bulkier

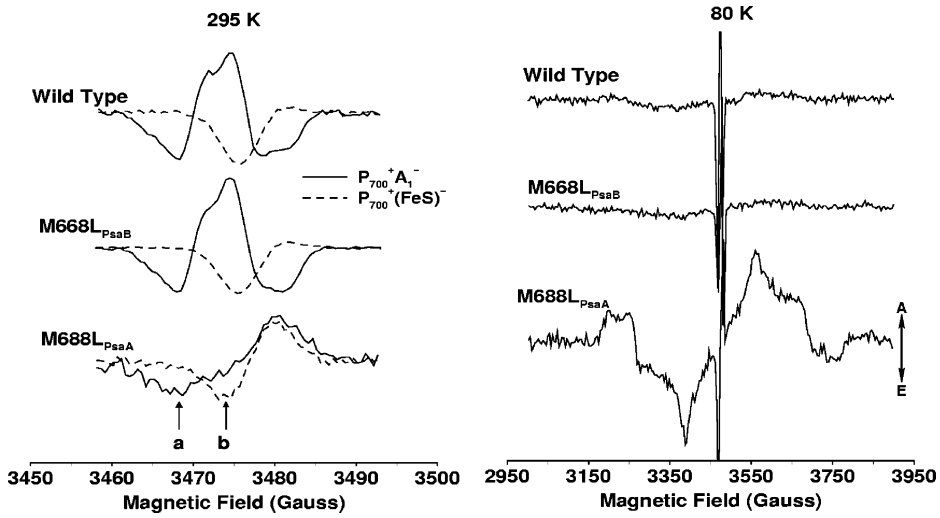

FIGURE 5: Room temperature and low-temperature spin polarized transient EPR spectra from the wild type (top), M668L$_{PsaB}$ (middle), and M688L$_{PsaA}$ (bottom) mutants. Left: Room temperature (295 K) spectra of the radical pair region at early time (solid curves, 60−160 ns) and late time (dashed curves, 1.2−1.6 μs). Right: Low temperature (80 K) spectra on a wide field scale to show the presence of triplet state spin polarization. The spectra represent integrated signal intensity in a time window from 0.25 to 1.4 μs. Positive amplitude corresponds to absorptive (A) and negative to emissive (E) EPR signals. Note the drastic change in all of the polarization patterns for the M688L$_{PsaA}$ mutant but not for the M668L$_{PsaB}$ mutant.

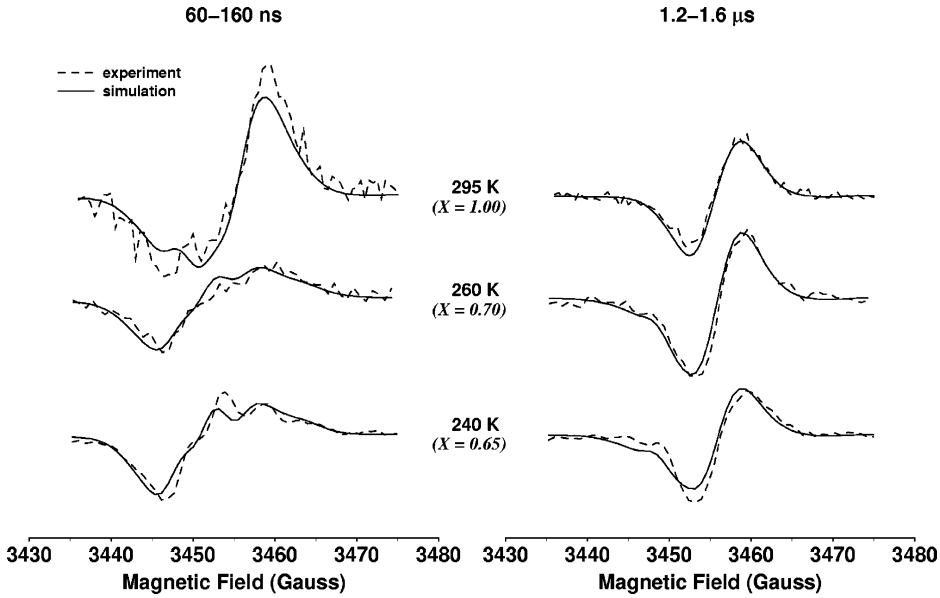

FIGURE 6: The temperature dependence of the spin polarization patterns from the M688L$_{PsaA}$ mutant. The spectra have been extracted from the time/field datasets as described in Figure 5 at temperatures 295, 260, 240 K. The dashed curves are simulations based on an admixture of reaction centers with short-lived and long-lived $P_{700}^+A_0^-$ according to eq 2. The parameter *X* is the fraction of centers with long-lived $P_{700}^+A_0^-$ and an effective lifetime of 2 ns is assumed for the reaction centers with long-lived $P_{700}^+A_0^-$. All other parameters and the algorithm used to calculate the spectra is given in detail in refs *34* and *35*. A single kinetic phase of forward electron transfer from A_1^- to F_X with a lifetime of 240 ns is assumed.

than that of Met, it is possible that the mutation causes disorder in the A_0 binding site. Thus, it is worth examining the effect that a distribution of electron-transfer rates would have. If the lifetime of A_0^- were sufficiently long, then charge recombination in the $P_{700}^+A_0^-$ state would outcompete forward electron transfer. Thus, a distribution of forward electron transfer rates should lead to back reaction in a fraction of the reaction centers. As the temperature is lowered, this fraction would likely increase. Thus, the temperature dependence of the spin polarization patterns may be due to a change in the distribution of A_0^- lifetimes in those reaction centers in which electron transfer to A_1 can occur.

To investigate this possibility, we have simulated the transient EPR data under the assumption that the distribution of A_0^- lifetimes is broad. The net polarization of P_{700}^+ and A_1^- due to spin dynamics during the lifetime of $P_{700}^+A_0^-$ is governed by the following expression (*34*, *35*):

$$p = qb/(\Omega^2 + k^2) \quad (1)$$

where $\Omega^2 = q^2 + b^2$, q is the difference in the precession frequencies of the spins on P_{700}^+ and A_0^-, (i.e., the frequency of the singlet−triplet mixing), $b = 2J + d$ is the flip-flop term of the spin−spin coupling, J is the exchange coupling, d is the dipolar coupling, and k is the mean decay rate for $P_{700}^+ A_0^-$. If the distribution of value of k is broad, then essentially all reaction centers will be in one of the two limiting cases $k^2 \gg \Omega^2$ or $k^2 \ll \Omega^2$. This type of behavior is

well-known for the dynamics of disordered systems (*36*) and has been used to describe the temperature dependence of the spectra of $^3P_{680}$ in PS II (*37*). Under these conditions, the observed spectrum is given approximately by

$$S = XS_{slow} + (1 - X)S_{fast} \quad (2)$$

where X is the fraction of reaction centers with $k^2 \ll \Omega^2$, S_{slow} is the spectrum corresponding to this limiting case, and S_{fast} is the spectrum in which the lifetime of $P_{700}{}^+A_0{}^-$ is sufficiently short that spin dynamics do not influence subsequent radical pairs (i.e., $p \approx 0$). The solid curves in Figure 6 show simulations of the spectra calculated on this basis using the parameters tabulated in ref *35* and using the procedure outlined in ref *38*. To represent the fraction with small k, we should also take into account the relative rates and quantum yields of singlet and triplet recombination. Since we do not have reasonable estimates of these values for the $M688L_{PsaA}$ mutant, we have simulated the room-temperature spectra by assuming a value of $X = 1$ and adjusted the value of k for the slow fraction. For the other temperatures, we have held the value of k fixed and adjusted the value of X. As can be seen, the temperature-dependent spectra are reproduced well by this procedure. Because of the uncertainty in parameters such as the spin−spin coupling and the recombination rates in the primary radical pair the values of X_{slow} and k only give a qualitative indication of the behavior. Nonetheless, the simulations show clearly that the changes induced by the mutations are described well as resulting from an increase in the effective lifetime of $A_0{}^-$ and that the temperature dependence can be attributed to a change in the relative weights of the two limiting case spectra. This analysis provides additional evidence that the lifetime of $A_0{}^-$ is altered by the mutation in the PsaA branch and strongly suggests that the mutation also induces disorder in the A_0 site.

Sample Variability in the PsaA-Side Mutant. To confirm the reliability and reproducibility of the above results, the measurements were repeated for three batches of PS I trimers isolated from independently grown cells. The whole cell growth studies of the mutant strain were also repeated. In particular, a considerable degree of variability in spin polarized EPR data was observed in the samples from the $M688L_{PsaA}$ mutant. This variability is demonstrated in Figures 7 and 8 for two extreme cases with considerably different triplet spectra at early time (Figure 7) and radical pair spectra (Figure 8). The top part of Figure 7 compares the triplet spectra taken in an early time window (0.25−1.4 μs), while corresponding spectra taken at late time (6−15 μs) are presented in the lower part of Figure 7. The experimental conditions are chosen such that the late spectrum due to a carotenoid triplet is the same in both samples (see below). The solid curves (sample 1) are from the same sample used for the results presented in Figures 4−6 and are measured at 220 K. The dashed curves are from a second sample measured at 80 K. The vertical bars labeled X, X′, Y, Y′, Z, and Z′ refer to the field positions corresponding to the canonical orientations of the chlorophyll *a* (^{3}Chl) triplet state (top) and the carotenoid (^{3}Car) triplet (bottom). Contributions from three species can be identified in the spectra: (i) the triplet state of P_{700} populated by radical pair recombination ($^3P_{700}$(RP)); (ii) antenna chlorophyll triplets populated by intersystem crossing (^{3}Chl *a* (ISC)); and (iii) antenna carotenoid triplets (^{3}Car) populated by triplet energy transfer from ^{3}Chl. Because $^3P_{700}$(RP) and ^{3}Chl *a* (ISC) are both monomeric chlorophyll *a* species at low temperature, their spectra have canonical resonances at the same field positions but their polarization patterns and kinetics differ.

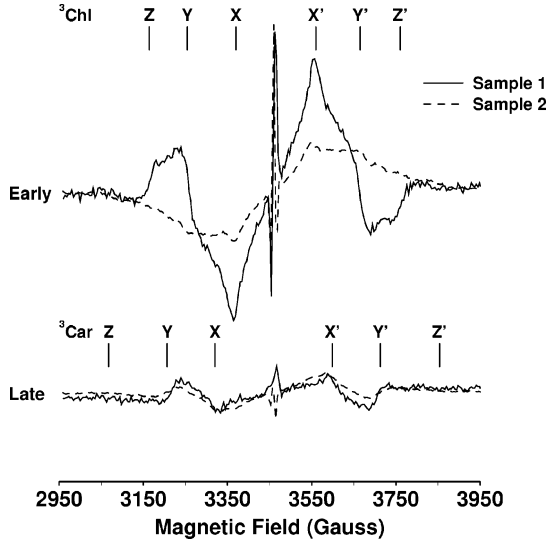

FIGURE 7: Comparison of the triplet spectra for PS I trimer samples prepared from two different sets of cell cultures of the $M688L_{PsaA}$ mutant. The vertical bars labeled X, Y, Z, etc. refer to the field positions at which the canonical orientations contribute to the triplet spectrum of chlorophyll *a* (upper marks) and a carotenoid with 9 conjugated double bonds in the polyene chain (lower marks). The spectra labeled "Early" are extracted from complete time/field scans in a time integration window of 0.25−1.4 μs, while those labeled "Late" correspond to a window from 7 to 15 μs. Note the dominance of the spectral contribution due to $^3P_{700}$ (RP) at early time in sample 1 but comparable spectra at late time due to ^{3}Car populated via energy transfer from ^{3}Chl populated by intersystem crossing (see text) in both samples.

The polarization patterns at early time (Figure 7, top) differ considerably for the two samples, but features are present at the field positions of the canonical Chl orientations in both spectra. For sample 1 (Figure 7, top, solid curve), the spectrum is clearly dominated by $^3P_{700}$(RP), while the pattern for sample 2 (Figure 7, top, dashed curve) is dominated by ^{3}Chl *a* (ISC). However, comparison of the experimental spectra with simulations (not shown) demonstrates that an admixture of $^3P_{700}$(RP) and ^{3}Chl *a* (ISC) patterns (with different weighting coefficients) is present in both samples. Similar admixtures have also been observed for the triplet spectra of spinach PS II particles and cyanobacterial PS II core particles (P. Tian, A. van der Est, and D. Stehlik, unpublished results). The patterns are very sensitive to an admixture of $^3P_{700}$(RP) and ^{3}Chl *a* (ISC) contributions at the Z canonical positions because the two species have opposite polarization in this region, and we estimate that the ratio $^3P_{700}$(RP)/^{3}Chl *a* (ISC) is about 4:1 for sample 1 but close to 1:1 for sample 2. An accurate determination of these ratios is complicated by the presence of carotenoid triplets, similar to those reported for the light harvesting complexes of purple bacteria (*39*) and also observed for PS II core particles and LHC II complexes (P. Tian, A. van der Est, and D. Stehlik, unpublished results). Because of its longer lifetime, the ^{3}Car signal can be kinetically separated and dominates the spectrum at late times (Figure 7, bottom). In the time window

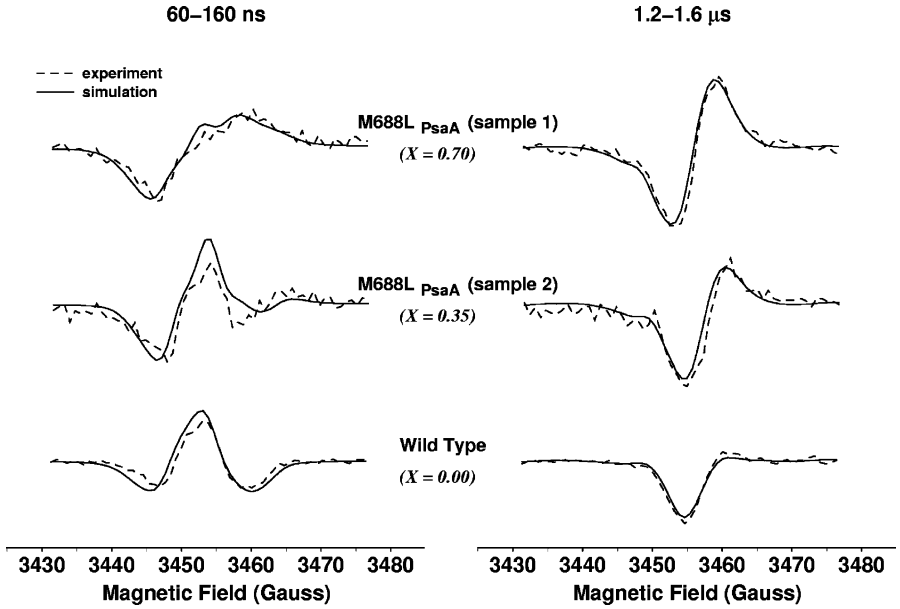

FIGURE 8: Comparison of the radical pair spectra at 260 K from the two samples of the $M688L_{PsaA}$ mutant (top and middle) and from the wild type (bottom). The dashed curves are the experimental spectra extracted from the data sets as described for Figure 5 and the solid curves are simulations based on the marked admixtures of long-lived and short-lived precursors as described in the caption to Figure 6.

Scheme 1: Proposed Energy and Kinetic Scheme for PS I[a]

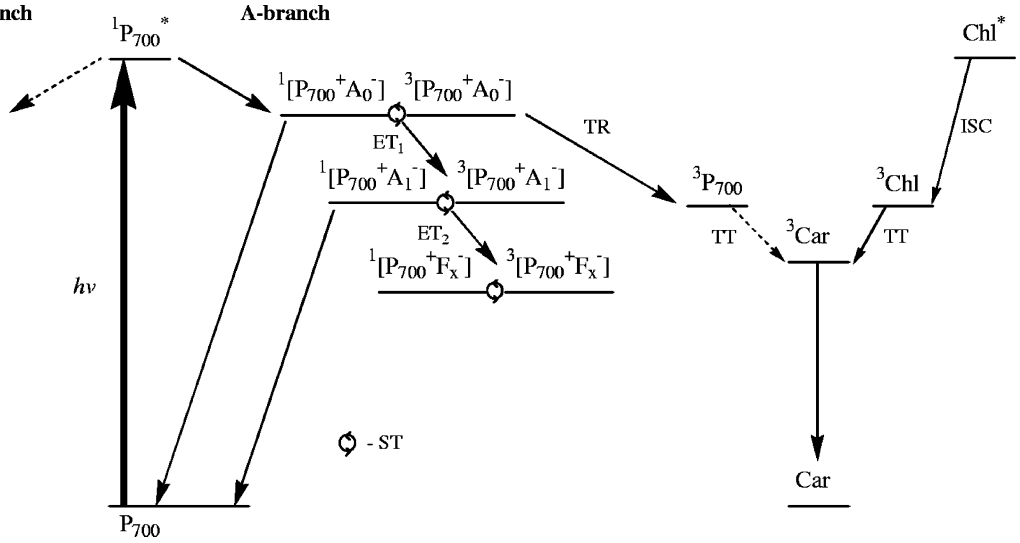

[a] TR: triplet radical pair recombination with characteristic spin polarization due to $\Delta m = 0$ selection. TT: triplet state transfer or trapping. ISC: intersystem crossing with zero-field spin selectivity. CS: primary charge separation. ET: spin conserving electron transfer. ET_{1t}: pure singlet electron transfer. ET_{1s}: ET comparable or larger than ST mixing time constant. ST: singlet−triplet mixing in radical pair state typical time constant: $\approx$ 0.5 ns. ET_2: secondary electron transfer from A_1 to iron sulfur centers, time constant 290 ns at room temperature.

shown in Figure 7 bottom only the X and Y canonical orientations are represented in the spectra because the spin relaxation is fast for the outer Z orientation. Hence, the features corresponding to the Z and Z′ canonical positions are more clearly recognized in the outer wings of the early spectrum Figure 7 (top). The separation between the outer edges of the carotenoid spectrum gives a value of ~39.5 mT for the zero field splitting parameter D, which is characteristic of carotenoids with nine conjugated double bonds in the polyene chain (*39*). This is consistent with the fact that the carotenoids in the X-ray structure of PS I (*1*, *2*) are best modeled as β-carotenoids (nine double bonds, with 17 out of 22 in trans configuration). As described previously by Frank et al. (*40*), the polarization pattern (E/A/E/A/E/A) is consistent with population of the carotenoid by triplet−triplet energy transfer from a chlorophyll triplet populated by intra-Chl *a* intersystem crossing. This assignment is supported by the saturation behavior, and spectral and kinetic properties of the optical absorbance changes presented in Figures 2 and 3, which also suggest the presence of a carotenoid triplet in the antenna.

From the relative intensities of the spectra in Figure 7, it is apparent that the main difference between the two samples is a considerable increase in the $^3P_{700}$(RP) contribution in sample 1 relative to the ^{3}Chl *a* (ISC) and ^{3}Car contributions (Scheme 1). As discussed above the temperature dependence of the radical pair polarization patterns can be simulated accurately under the assumption of a distribution of forward electron-transfer rates. If this model is correct, then the large difference in the intensity of the $^3P_{700}$(RP) between sample

1 and sample 2 suggests a different distribution of forward electron-transfer rates in the two samples. Indeed, if the mutation leads to disorder in the A_0 site, then such variability between samples is expected. We have investigated this idea further by simulating the $P_{700}^+A_1^-$ radical pair spectra of the two samples at 260 K. The results are shown in Figure 8 and are presented in the same manner as the temperature-dependent spectra in Figure 5. There is a significant difference between the spectra for the two samples of PsaA side mutants, but both are different from the wild type (Figure 8, bottom). Again, all of the spectra can be satisfactorily reproduced using the model of a broad distribution of A_0^- lifetimes. The simulations show that the spectra of sample 2 correspond to a much smaller fraction of reaction centers with slow forward electron transfer at 260 K compared to sample 1. Consistent with this behavior, a much smaller yield of charge recombination to $^3P_{700}$ is observed at 80 K for this sample. Hence the data suggest that the $M688L_{PsaA}$ mutation slows down the electron transfer from A_0 to A_1 and leads to a distribution of lifetimes for the $P_{700}^+A_0^-$ state. Moreover, this distribution may vary from sample to sample.

Such a preparation-dependent distribution could be the result of structural instability in the A_0 environment induced by the mutation. It should be noted that this proposed instability in the PsaA-side mutant does not lead to variability in the yield of charge separation between P_{700} and the iron-sulfur clusters at room temperature. However, in the context of the activity of the two branches, the most important result is that no such effects are observed for the samples of the PsaB mutant, which consistently show wild-type levels of charge separation to the iron−sulfur clusters. Since the PsaB-side A_0 site is expected to be similarly destabilized by the Met-to-Leu mutation, we are once again left with the conclusion that either electron transfer along the PsaB-side is either insignificant or that it is ineffective in generating spin-polarized transient EPR signals.

DISCUSSION

The most important current issue related to the function of PS I is the extent to which each of the two branches of cofactors is active in light-induced electron transfer. While a unidirectional scheme appears to be functionally required in Type II reaction centers (bacterial reaction centers or PS II), such a requirement is not necessary in Type I reaction centers, where the two branches diverge at a common primary donor and reconverge at the iron-sulfur clusters that serve as the terminal electron acceptors. A spectroscopic observable for electron transfer through either the PsaA-branch or the PsaB-branch does not exist in PS I, because all of the primary cofactors (P_{700}, A_{-1}, and A_0) are Chl *a* molecules, as are the 90 antenna molecules. Selective observation of P_{700}, A_{-1}, and A_0 via ultrafast kinetics and absorption difference spectroscopy is possible, in principle, but in practice the application of this technique is complicated by the strong spectral and kinetic overlap of absorbance changes associated with the antenna chlorophylls in PS I. In the wild type at 295 K, kinetics of about 1 ps have been measured for the first charge separation step (as well as the A_0^- rise time), and 10−50 ps have been measured for the A_0^- to A_1 step (*41*−*44*).

The subsequent electron transfer from A_1^- to F_X is more easily measured and has provided the majority of data related to the issue of directionality in PS I. At ambient temperatures, the rate of this step is found to be biexponential with fast (10−30 ns) and slow (200−300 ns) kinetic phases (*38*). Studies of site-directed mutants in the A_1 environment clearly identify the slow phase with electron transfer along the PsaA branch (*3*−*5*, *7*−*9*). The assignment of the fast kinetic phase is still under debate. Optical data of site-directed point mutants show a correlation between mutations in the PsaB branch and changes in the kinetics of the fast phase (*4*, *8*). However, a recent study of stromal subunit deletion mutants (*38*) showed that removal of PsaF, which interacts strongly with the PsaA-branch quinone binding region, but not with P_{700}, also induces a fast kinetic phase.

The most striking result found here is that, while the $M668L_{PsaB}$ has no discernible effect on properties associated with forward electron transfer, the $M688L_{PsaA}$ mutation causes dramatic changes. These changes include (i) slower growth rates, higher light sensitivity, and reduced amounts of PS I; (ii) a reduced yield of electron transfer from P_{700} to the F_A/F_B iron-sulfur clusters at room temperature; (iii) a concomitant contribution from the $^3P_{700}$ triplet state due to $P_{700}^+A_0^-$ recombination; and (iv) a change in the intensity and shape of the polarization patterns of the consecutive radical pair states $P_{700}^+A_1^-$ and $P_{700}^+F_X^-$ in the PsaA-side mutant compared with the wild type and the PsaB-side mutant. The most straightforward interpretation of these results is that electron transfer occurs primarily along the PsaA branch of cofactors. Since the environments of the two A_0 chlorophyll molecules are nearly identical, these results provide evidence for strongly asymmetric electron-transfer activity in cyanobacterial PS I. However, care must be taken in interpreting the results in terms of minor electron-transfer activity along the PsaB-branch because none of the experimental methods currently used can guarantee the detection of the entire population of photoactive PS I complexes. This conclusion therefore does not exclude some minor fraction of electron transfer along the PsaB-branch. Confirmation of the EPR results by other methods is still required. Nevertheless, all data presented in this work are consistent with asymmetric electron transfer along the PsaA-branch in cyanobacterial PS I.

For the $M688L_{PsaA}$ and $M668L_{PsaB}$ mutants, both ultrafast and nanosecond optical absorbance data will provide an important complement to the data presented here. The ultrafast experiments will allow the proposal that PsaA-branch mutation leads to a slowing of the forward electron-transfer passed A_0 to be tested, while the relative amplitudes of the two phases of A_1^- reoxidation can be compared with nanosecond optical absorbance difference measurements. Experiments of this type are in progress and will be presented in a forthcoming paper.

After submission of this paper, a similar study by Fairclough et al. (*6*) on histidine mutants of the corresponding Met residues in PS I from *C. rheinhardtii* was published. It was concluded that a large fraction of electrons proceed along the PsaB-branch, and that electron transfer in the PsaA-branch may not be necessary for photoautrophic growth under aerobic conditions. These conclusions are based largely on the absence of an out-phase-echo signal at 265 K in the PsaA-side mutant. However, it should be noted that in contrast to transient EPR, which measures the entire spin polarization, the out-of-phase echo is sensitive only to the

dipolar order in the spin system. Because singlet−triplet mixing in the precursor leads to loss of dipolar order, it also leads to loss of the out-of-phase echo. Hence, the absence of an out-of-phase echo such as reported in ref *6* does not necessarily indicate loss of electron transfer. The conclusions in ref *6* are also based on the appearance of signals assigned to reduced Q_K-B. We have performed many of the same experiments on the $M688L_{PsaA}$ and $M668L_{PsaB}$ mutants in *Synnechocystis* sp. PCC 6803 and have found none of these features in the EPR data. In particular, we find no difference in the decay of the electron spin polarization due to relaxation in the two Leu mutants. It is possible that this difference is because a eukaryotic organism was used (*6*) while the data here are from a cyanobacterium. Indeed, early attempts to measure the rate of A_1^- to F_X electron transfer yielded conflicting results because the eukaryotic PS I samples showed mostly the fast phase (*45*) while only the slow phase could be detected in the cyanobacterial samples (*46*, *47*). Hence, further experiments and a direct comparison of the two species under identical conditions are needed to gain a better understanding of such possible differences.

ACKNOWLEDGMENT

The authors thank Ms. Yumiko Sakuragi for helpful advice on measuring phylloquinone by HPLC and Dr. David Becker for a critical reading of the manuscript.

REFERENCES

1. Fromme, P., Jordan, P., and Krauss, N. (2001) Structure of Photosystem I. *Biochim. Biophys. Acta 1507*, 5−31.
2. Jordan, P., Fromme, P., Witt, H. T., Klukas, O., Saenger, W., and Krauss, N. (2001) Three-dimensional structure of cyanobacterial Photosystem I at 2.5 angstrom resolution. *Nature 411*, 909−917.
3. Boudreaux, B., MacMillan, F., Teutloff, C., Agalarov, R., Gu, F. F., Grimaldi, S., Bittl, R., Brettel, K., and Redding, K. (2001) Mutations in both sides of the Photosystem I reaction center identify the phylloquinone observed by electron paramagnetic resonance spectroscopy. *J. Biol. Chem. 276*, 37299−37306.
4. Guergova-Kuras, M., Boudreaux, B., Joliot, A., Joliot, P., and Redding, K. (2001) Evidence for two active branches for electron transfer in Photosystem I. *Proc. Natl. Acad. Sci. U.S.A. 98*, 4437−4442.
5. Muhiuddin, I. P., Heathcote, P., Carter, S., Purton, S., Rigby, S. E. J., and Evans, M. C. W. (2001) Evidence from time-resolved studies of the $P700^{\bullet+}/A_1^{\bullet-}$ radical pair for photosynthetic electron transfer on both the PsaA and PsaB branches of the Photosystem I reaction centre. *FEBS Lett. 503*, 56−60.
6. Fairclough, W. V., Forsyth, A., Evans, M. C. W., Rigby, S. E. J., Purton, S., and Heathcote, P. (2003) Bidirectional electron transfer in Photosystem I: electron transfer on the PsaA side is not essential for phototrophic growth in *Chlamydomonas*. *Biochim. Biophys. Acta 1606*, 43−55.
7. Golbeck, J., Xu, W., Zybailov, B., van der Est, A., Pushkar, J., Zech, S., Stehlik, D., and Chitnis, P. (2001) Electron-Transfer Through the Quinone Electron Acceptor in Photosystem I in *PS2001: 12th International Congress on Photosynthesis* (Chritchley, C., Ed.), CSIRO Publishing, Melbourne Australia, Brisbane, Australia.
8. Xu, W., Chitnis, P. R., Valieva, A., van der Est, A., Brettel, K., Guergova-Kuras, M., Pushkar, Y. N., Zech, S. G., Stehlik, D., Shen, G., Zybailov, B., and Golbeck, J. H. (2003) Electron transfer in cyanobacterial Photosystem I: II. Determination of forward electron-transfer rates of site-directed mutants in a putative electron-transfer pathway from A_0 through A_1 to F_X. *J. Biol. Chem. 278*, 27876−27887.
9. Xu, W., Chitnis, P., Valieva, A., van der Est, A., Pushkar, Y. N., Krzystyniak, M., Teutloff, C., Zech, S. G., Bittl, R., Stehlik, D., Zybailov, B., Shen, G., and Golbeck, J. H. (2003) Electron transfer in cyanobacterial Photosystem I: I. Physiological and spectroscopic characterization of site-directed mutants in a putative electron-transfer pathway from A_0 through A_1 to F_X. *J. Biol. Chem. 278*, 27864−27875.
10. Yang, F., Shen, G. Z., Schluchter, W. M., Zybailov, B. L., Ganago, A. O., Vassiliev, I. R., Bryant, D. A., and Golbeck, J. H. (1998) Deletion of the PsaF polypeptide modifies the environment of the redox-active phylloquinone A_1. Evidence for unidirectionality of electron transfer in Photosystem I. *J. Phys. Chem. B 102*, 8288−8299.
11. Moser, C. C., Keske, J. M., Warncke, K., Farid, R. S., and Dutton, P. L. (1992) Nature of biological electron-transfer. *Nature 355*, 796−802.
12. Shen, G. Z., Zhao, J. D., Reimer, S. K., Antonkine, M. L., Cai, Q., Weiland, S. M., Golbeck, J. H., and Bryant, D. A. (2002) Assembly of Photosystem I. I. Inactivation of the *rubA* gene encoding a membrane-associated rubredoxin in the cyanobacterium *Synechococcus* sp PCC 7002 causes a loss of Photosystem I activity. *J. Biol. Chem. 277*, 20343−20354.
13. MacKinney, G. (1941) Absorption of light by chlorophylls. *J. Biol. Chem. 140*, 315−322.
14. Lichtenthaler, H. K. (1987) Chlorophylls and carotenoids: pigments of photosynthetic membranes. *Methods Enzymol. 148*, 350−382.
15. Cunningham, F. X., Jr., Sun, Z., Chamovitz, D., Hirschberg, J., and Gantt, E. (1994) Molecular structure and enzymatic function of lycopene cyclase from the cyanobacterium *Synechococcus* sp strain PCC7942. *Plant Cell 6*, 1107−1121.
16. Johnson, T. W., Shen, G. Z., Zybailov, B., Kolling, D., Reategui, R., Beauparlant, S., Vassiliev, I. R., Bryant, D. A., Jones, A. D., Golbeck, J. H., and Chitnis, P. R. (2000) Recruitment of a foreign quinone into the A_1 site of Photosystem I−I. Genetic and physiological characterization of phylloquinone biosynthetic pathway mutants in *Synechocystis* sp PCC 6803. *J. Biol. Chem. 275*, 8523−8530.
17. Vassiliev, I. R., Antonkine, M. L., and Golbeck, J. H. (2001) Iron−sulfur clusters in Type I reaction centers. *Biochim. Biophys. Acta 1507*, 139−160.
18. Joliot, P., Beal, D., and Frilley, B. (1980) A new spectrophotometric method for the study of photosynthetic reactions. *J. Chim. Phys.-Chim. Biol. 77*, 209−216.
19. Kramer, D. M., and Sacksteder, C. A. (1998) A diffused-optics flash kinetic spectrophotometer (DOFS) for measurements of absorbance changes in intact plants in the steady-state. *Photosyn. Res. 56*, 103−112.
20. van der Est, A., Hager-Braun, C., Leibl, W., Hauska, G., and Stehlik, D. (1998) Transient electron paramagnetic resonance spectroscopy on green-sulfur bacteria and heliobacteria at two microwave frequencies. *Biochim. Biophys. Acta 1409*, 87−98.
21. Shen, G. Z., Boussiba, S., and Vermaas, W. F. J. (1993) *Synechocystis* sp. PCC 6803 strains lacking Photosystem I and phycobilisome function. *Plant Cell 5*, 1853−1863.
22. Vassiliev, I. R., Jung, Y. S., Mamedov, M. D., Semenov, A. Y., and Golbeck, J. H. (1997) Near-IR absorbance changes and electrogenic reactions in the microsecond-to-second time domain in Photosystem I. *Biophys. J. 72*, 301−315.
23. Hiyama, T., and Ke, B. (1972) Difference spectra and extinction coefficients of P700. *Biochim. Biophys. Acta 267*, 160−171.
24. Semenov, A. Y., Vassiliev, I. R., van der Est, A., Mamedov, M. D., Zybailov, B., Shen, G. Z., Stehlik, D., Diner, B. A., Chitnis, P. R., and Golbeck, J. H. (2000) Recruitment of a foreign quinone into the A_1 site of Photosystem I − Altered kinetics of electron transfer in phylloquinone biosynthetic pathway mutants studied by time-resolved optical, EPR, and electrometric techniques. *J. Biol. Chem. 275*, 23429−23438.
25. Schlodder, E., Paul, A., and Cetin, M. (2001) in *PS2001: 12th International Congress on Photosynthesis* (Critchley, C., Ed.) pp S6−015, CSIRO Publishers Melbourne Australia, Brisbane Australia.
26. Benasson, R. V., Dawe, E. A., Long, D. A., and Land, E. J. (1977) Singlet → triplet intersystem crossing quantum yields of photosynthetic and related polyene. *J. Chem. Soc., Faraday Trans. 73*, 1319−1325.
27. van der Est, A., Bock, C., Golbeck, J., Brettel, K., Sétif, P., and Stehlik, D. (1994) Electron transfer from acceptor A_1 to the iron−sulfur centers in Photosystem I as studied by transient EPR spectroscopy. *Biochemistry 33*, 11789−11797.
28. Schlodder, E., Falkenberg, K., Gergeleit, M., and Brettel, K. (1998) Temperature dependence of forward and reverse electron transfer from A_1^-, the reduced secondary electron acceptor in Photosystem I. *Biochemistry 37*, 9466−9476.

29. Agalarov, R., and Brettel, K. (2003) Temperature dependence of biphasic forward electron transfer from the phylloquinone(s) A_1 in Photosystem I: only the slower phase is activated. *Biochim. Biophys. Acta 1604*, 7−12.
30. Budil, D. E., and Thurnauer, M. C. (1991) The chlorophyll triplet-state as a probe of structure and function in photosynthesis. *Biochim. Biophys. Acta 1057*, 1−41.
31. Frank, H. A., McLean, M. B., and Sauer, K. (1979) Triplet states in Photosystem I of spinach chloroplasts and subchloroplast particles. *Proc. Natl. Acad. Sci. U.S.A. 76*, 5124−5128.
32. Sieckmann, I., Brettel, K., Bock, C., van der Est, A., and Stehlik, D. (1993) Transient electron-paramagnetic-resonance of the triplet-state of P700 in Photosystem. 1. Evidence for triplet delocalization in room-temperature. *Biochemistry 32*, 4842−4847.
33. Pushkar, Y. N., Zech, S. G., Stehlik, D., Brown, S., van der Est, A., and Zimmermann, H. (2002) Orientation and protein−cofactor interactions of monosubstituted *n*-alkyl naphthoquinones in the A_1 binding site of Photosystem I. *J. Phys. Chem. B 106*, 12052−12058.
34. Kandrashkin, Y. E., Salikhov, K. M., van der Est, A., and Stehlik, D. (1998) Electron spin polarization in consecutive spin-correlated radical pairs: Application to short-lived and long-lived precursors in Type 1 photosynthetic reaction centres. *Appl. Magn. Res. 15*, 417−447.
35. Kandrashkin, Y. E., Vollmann, W., Stehlik, D., Salikhov, K., and van der Est, A. (2002) The magnetic field dependence of the electron spin polarization in consecutive spin correlated radical pairs in Type I photosynthetic reaction centres. *Mol. Phys. 100*, 1431−1443.
36. Rössler, E., Taupitz, M., Borner, K., Schulz, M., and Vieth, H. M. (1990) A simple method analyzing H-2 nuclear-magnetic-resonance line- shapes to determine the activation-energy distribution of mobile guest molecules in disordered-systems. *J. Chem. Phys. 92*, 5847−5855.
37. Kamlowski, A., Frankemoller, L., van der Est, A., Stehlik, D., and Holzwarth, A. R. (1996) Evidence for delocalization of the triplet state $^3P_{680}$ in the $D_1D_2cyt_b559$-complex of Photosystem II. *Ber. Bunsen-Ges. Phys. Chem. Chem. Phys. 100*, 2045−2051.
38. van der Est, A., Valieva, A., Kandrashkin, Y. E., Shen, G., Bryant, D. A., and Golbeck, J. (2004) Removal of PsaF alters forward electron transfer in Photosystem I: Evidence for fast reoxidation of Q_K-A in subunit deletion mutants of *Synechococcus* sp. PCC 7002. *Biochemistry 43*, 1264−1275.
39. Bittl, R., Schlodder, E., Geisenheimer, I., Lubitz, W., and Cogdell, R. J. (2001) Transient EPR and absorption studies of carotenoid triplet formation in purple bacterial antenna complexes. *J. Phys. Chem. B 105*, 5525−5535.
40. Frank, H. A., Bolt, J. D., Costa, S., and Sauer, K. (1980) Electron-paramagnetic resonance detection of carotenoid triplet-states. *J. Am. Chem. Soc. 102*, 4893−4898.
41. Nuijs, A. M., Shuvalov, V. A., van Gorkom, H. J., Plijter, J. J., and Duysens, L. N. M. (1986) Picosecond absorbency difference spectroscopy on the primary reactions and the antenna-excited states in Photosystem I particles. *Biochim. Biophys. Acta 850*, 310−318.
42. Shuvalov, V. A., Nuijs, A. M., Van Gorkom, H. J., Smit, H. W. J., and Duysens, L. N. M. (1986) Picosecond absorbency changes Upon selective excitation of the primary electron-donor P700 in Photosystem I. *Biochim. Biophys. Acta 850*, 319−323.
43. Hastings, G., Kleinherenbrink, F. A. M., Lin, S., McHugh, T. J., and Blankenship, R. E. (1994) Observation of the reduction and reoxidation of the primary electron acceptor in Photosystem-I. *Biochemistry 33*, 3193−3200.
44. Savikhin, S., Xu, W., Martinsson, P., Chitnis, P. R., and Struve, W. S. (2001) Kinetics of charge separation and $A_0^- \rightarrow A_1$ electron transfer in photosystem I reaction centers. *Biochemistry 40*, 9282−9290.
45. Mathis, P., and Sétif, P. (1988) Kinetic studies on the function of A_1 in the Photosystem I reaction center. *FEBS Lett. 237*, 65−68.
46. Bock, C. H., van der Est, A. J., Brettel, K., and Stehlik, D. (1989) Nanosecond electron-transfer kinetics in Photosystem-I as obtained from transient EPR at room-temperature. *FEBS Lett. 247*, 91−96.
47. Brettel, K. (1988) Electron transfer from A_1^- to an iron−sulfur center with $t_{1/2} = 200$ ns at toom temperature in Photosystem-I - Characterization by flash absorption spectroscopy. *FEBS Lett. 239*, 93−98.

BI035633F